A modeling study of the effect of nitric acid on cloud properties

Huiwen Xue and Graham Feingold
Environmental Technology Laboratory, NOAA, Boulder, Colorado, USA

Received 9 March 2004; revised 25 June 2004; accepted 13 July 2004; published 23 September 2004.

[1] The effect of nitric acid (HNO_3) on cloud microphysical and radiative properties is studied using an adiabatic cloud parcel model for a range of aerosol size distributions, different water vapor mass accommodation coefficients, and HNO_3 concentrations. Results show that HNO_3 not only increases cloud drop number concentration N_d, but also leads to significantly broader droplet size spectra at both the small- and large-size ends. The broader spectra are generally the result of competition for H_2O and HNO_3 among the polydisperse droplets. The increase in the number of activated cloud droplets in the presence of HNO_3, and the deactivation of some of the small cloud droplets due to the outgasing of HNO_3, lead to spectral broadening at the small-size end. At the large-size end the broadening is caused by an increase in the driving force for growth. For small drops the driving force tends to be decreased by the presence of HNO_3. Although N_d increases with increasing HNO_3 concentration, the increases in cloud optical depth and albedo due to HNO_3 cannot necessarily be predicted by the commonly used relationships for cloud optical properties. The dependence of the cloud optical depth on N_d to the one-third power is shown to be an overestimate because droplet spectra are significantly broadened by HNO_3. We show that broadening effects due to HNO_3 and other chemical or microphysical factors need to be considered when estimating cloud optical properties and their effect on climate. *INDEX TERMS:* 0305 Atmospheric Composition and Structure: Aerosols and particles (0345, 4801); 0320 Atmospheric Composition and Structure: Cloud physics and chemistry; 1610 Global Change: Atmosphere (0315, 0325); *KEYWORDS:* cloud droplets, nitric acid, aerosol indirect effect

Citation: Xue, H., and G. Feingold (2004), A modeling study of the effect of nitric acid on cloud properties, *J. Geophys. Res.*, *109*, D18204, doi:10.1029/2004JD004750.

1. Introduction

[2] Increased aerosol concentrations due to anthropogenic activities can lead to higher cloud droplet concentrations and thereby enhance cloud albedo (the first aerosol indirect effect or Twomey effect) [*Twomey*, 1974, 1977]. To assess the aerosol indirect effect, a robust connection is needed between global aerosol properties and global cloud properties. *Twomey* [1977] originally described the relationship between cloud drop number concentration N_d and aerosol number concentration N_a considering a fixed liquid water content (LWC). In the intervening decades studies of the aerosol indirect effect have considered the broader implications of the effects of aerosol on the cloud system including cloud dynamical evolution and feedbacks [e.g., *Albrecht*, 1989; *Rosenfeld*, 2000; *Schwartz et al.*, 2002; *Feingold*, 2003], and at a range of scales. The goal of these studies is to consider possible changes in cloud properties that result in changes in cloud albedo, the modification of ice and water clouds, precipitation patterns and rates, and the composition of the atmosphere.

[3] More recently it has been noted that in addition to aerosol size and composition effects on cloud microphysics, some "chemical factors" may also produce more cloud droplets and impose additional cooling effect on the climate. These chemical factors include highly soluble trace gases, slightly soluble solute, and surface tension depression due to organic compounds [e.g., *Facchini et al.*, 1999; *Charlson et al.*, 2001]. Most of these chemical factors result in an increase in droplet concentration, all other conditions being equal. A chemical factor that may lead to fewer cloud droplets and hence a warming effect on the climate is the growth retardation of some droplets due to film-forming organic compounds on the droplet surface [*Feingold and Chuang*, 2002]. Aqueous-phase chemical processing of aerosol that has participated as cloud condensation nuclei (CCN) can also lead to a bimodal size distribution after the cloud evaporates [*Hoppel et al.*, 1994]. In the next cloud cycle, N_d may either be increased or reduced, depending on the circumstances, and impose either a cooling or a warming effect on climate [*Feingold and Kreidenweis*, 2000].

[4] From the perspective of the aerosol indirect effect in warm clouds, HNO_3 is considered to be the most important of the highly soluble trace gases in the atmosphere [*Charlson et al.*, 2001]. The effect of HNO_3 on cloud formation has been studied over the past decade to better understand the cloud radiative forcing. As discussed by *Kulmala et al.* [1997] and *Laaksonen et al.* [1998], dissolution of HNO_3 in water droplets results in the addition of solute in growing haze particles. It is therefore easier for these particles to transform into cloud droplets. Consistent

results from adiabatic cloud parcel model simulations have shown that HNO_3 produces more cloud droplets [*Kulmala et al.*, 1993, 1995, 1996; *Hegg*, 2000; *Nenes et al.*, 2002]. When compared to baseline simulations without HNO_3, cloud droplet concentration can be increased by almost 60% when 5 ppb HNO_3 is initially in the gas phase and cloud updrafts are on the order of 0.1 m s^{-1}. This increase is comparable to the increase in N_d when the aerosol number concentration is doubled [e.g., *Nenes et al.*, 2002].

[5] However, as will be shown here, knowing the change in N_d is not sufficient to predict the change in cloud radiative properties because changes in the breadth of the droplet spectrum often accompany changes in N_d [*Feingold et al.*, 1997; *Ackerman et al.*, 2000; *Liu and Daum*, 2002].

[6] Field observation of broader drop spectra associated with higher N_d is well known [*Martin et al.*, 1994; *Gerber*, 1996]. Physically (i.e., without considering chemical effects), this could be caused by the competition for water vapor by more drops when the air contains more aerosol particles. Because growth by condensation of water vapor tends to result in a narrowing of the drop size distribution, the increased competition results in diminished growth per drop, and therefore less narrowing. *Liu and Daum* [2002] calculated the climate forcing due to this effect to be $-0.19 \sim -0.93$ W m^{-2} for an increase of 15% in N_d at $N_d = 100$ cm^{-3}, i.e., smaller than the -1.03 W m^{-2} forcing calculated for the Twomey effect alone [*Charlson et al.*, 1992]. Thus the aerosol indirect effect is likely overestimated when not considering spectral broadening. The broadened spectra lead to lower cloud susceptibility (a change in albedo for a change in drop concentration) compared to *Twomey*'s [1991] original assessment. *Ackerman et al.* [2000] showed that although Twomey's parameterization of cloud susceptibility represents well the measurements in ship tracks, the agreement may be fortuitous due to offsetting effects from changes in several parameters, including LWC, the breadth of the droplet size distributions, and cloud thickness. On a global scale, the spectral broadening effect has been considered in the study of *Peng and Lohmann* [2003] in a general circulation model and the results agree with satellite data better than they would have without considering this effect. However, it is not clear that the satellite retrievals are robust enough to conclude that spectral broadening is indeed the reason for the improved agreement.

[7] Unlike the condensation process, collision-coalescence reduces drop concentration and broadens drop spectra. Using a range of cloud models, *Feingold et al.* [1997] showed that when spectral broadening is accompanied by a decrease in N_d (e.g., due to collision-coalescence) the decrease in cloud albedo is larger than it would have been without the consideration of spectral broadening. Clouds also have higher susceptibility. *McFarquhar and Heymsfield* [2001] used INDOEX measurements to provide a new susceptibility parameterization for clouds experiencing collision-coalescence by taking into account the changes in cloud spectral breadth and found that the susceptibility is two times larger than that calculated using the original Twomey definition, in agreement with *Feingold et al.* [1997].

[8] This paper will address the increase in N_d and the associated drop spectral broadening resulting from uptake of HNO_3, and its effects on cloud effective radius, optical depth and albedo. The focus will be on the physical mechanisms behind spectral broadening due to HNO_3. In addition, because the mass accommodation coefficient of water has large uncertainties, but its magnitude is important in cloud microphysics [*Zou and Fukuta*, 1999; *Hudson and Yum*, 1997], this paper will also address the sensitivity of model results to the mass accommodation coefficient of water.

[9] To do so, cloud formation is simulated using an adiabatic parcel model for different updraft velocities, HNO_3 concentrations, water vapor mass accommodation coefficients, and initial aerosol size distributions. Cloud optical properties evaluated with and without the spectral broadening effect will be compared. In section 2, theory of droplet equilibrium and growth and some simplified theory of cloud radiative properties will be discussed. Section 3 will present parcel model results and discussion. The conclusions will be presented in section 4.

2. Theory

2.1. Droplet Equilibrium and Growth

[10] The traditional Köhler theory describes the equilibrium water vapor pressure over droplet surfaces [*Pruppacher and Klett*, 1997, p. 173],

$$S_{sfc} \approx 1 + \frac{a}{r} - \frac{b}{r^3}, \tag{1}$$

where S_{sfc} is the water saturation ratio at the drop surface, r is the radius of the droplet, a/r is a term describing the increase of surface vapor pressure due to the curvature, and b/r^3 is a term describing the decrease of surface vapor pressure due to the dissolved solute. The diffusive growth rate of a cloud droplet has the form [e.g., *Pruppacher and Klett*, 1997, p. 511],

$$r\frac{dr}{dt} = \frac{e_s(T)\left(S_{amb} - S_{sfc}\right)}{\frac{\rho_w RT}{D^* M_w} + \frac{L\rho_w e_s(T)}{k^* T}\left(\frac{LM_w}{RT} - 1\right)}, \tag{2}$$

where $e_s(T)$ is the equilibrium vapor pressure over a flat surface at the ambient air temperature T, S_{amb} the saturation ratio of the ambient air, ρ_w the density of the droplet, R the universal gas constant, M_w the molecular weight of water, and L the latent heat of water condensation; D^* and k^* are respectively the effective diffusion coefficient of water vapor in air and the effective thermal conductivity of air, including kinetic effects. The driving force for droplet growth (or evaporation) is defined as $S_{amb} - S_{sfc}$.

[11] When highly soluble gases, such as HNO_3, are produced in the atmosphere, they can contribute solute to the droplets, hence lower the water vapor pressure over the droplet surface and lead to enhanced growth. To quantify the equilibrium water vapor pressure of a solution containing HNO_3, *Clegg et al.* [1998] developed a thermodynamic model for the NH_4^+-H^+-SO_4^{2-}-NO_3^--H_2O system that can be used to study the effect of HNO_3 on the activation and growth of ammonium (bi)sulfate, the most relevant atmospheric aerosols. The model provides the water activity of a solution with given concentrations of ions at tropospheric temperatures.

[12] The transport of HNO_3 to the droplet surface is governed by the same theory as that for water vapor. Assuming HNO_3 does not react inside the droplets and the liquid-phase HNO_3 concentration C_{aq} is uniform, the transport rate of HNO_3 can be written as [*Seinfeld and Pandis*, 1998, p. 634]

$$\frac{dC_{aq}}{dt} = k_{mt}\left(\frac{p}{RT} - \frac{C_{aq}}{H_A RT}\right), \tag{3}$$

where k_{mt} is the mass transport coefficient of HNO_3 including the gas-phase diffusion and the kinetic effect, p the vapor pressure of HNO_3 in the ambient air, and H_A the effective Henry's law coefficient of HNO_3.

2.2. Cloud Radiative Properties

[13] Cloud droplet effective radius is defined as

$$r_e = \frac{\int_0^\infty r^3 n(r)dr}{\int_0^\infty r^2 n(r)dr}, \tag{4}$$

where $n(r)$ is the droplet size distribution. Past studies have parameterized r_e in terms of the cloud LWC and N_d. The cloud LWC can be calculated from the droplet size distribution as

$$L = \frac{4}{3}\pi\rho_w \int_0^\infty r^3 n(r)dr = \frac{4}{3}\pi\rho_w N_d \overline{r^3}, \tag{5}$$

where $4/3\ \pi\overline{r^3}$ is the average volume of the droplets. With the mean volume radius r_v defined as $r_v^3 = \overline{r^3}$, equation (5) takes the form

$$L = \frac{4}{3}\pi\rho_w N_d r_v^3. \tag{6}$$

[14] If a relationship exists between r_v and r_e, equation (6) can be used to parameterize r_e in terms of LWC and N_d. *Martin et al.* [1994] indicated that there is a linear relationship between r_v and r_e in stratocumulus clouds where little entrainment occurs,

$$r_v^3 = k r_e^3, \tag{7}$$

where k is a constant representing the shape of the droplet spectrum, and is related to the relative spectral dispersion (D) and the coefficient of skewness (a). The authors pointed out that k will be affected much more by changes in D than changes in a so that the constant k can be written as

$$k \approx \frac{(1+D^2)^3}{(1+3D^2)^2}, \tag{8}$$

with k inversely proportional to D if $D^2 < 1$. By using equations (6) and (7), r_e may be parameterized as

$$r_e = \left(\frac{3L}{4\pi\rho_w k N_d}\right)^{1/3}. \tag{9}$$

It is seen that r_e is a function of both N_d and k to the one-third power. Considering constant LWC, the change in r_e due to the changes in N_d and k can be expressed as

$$\frac{r_e}{r_{e0}} = \left(\frac{k}{k_0}\right)^{-1/3}\left(\frac{N_d}{N_{d0}}\right)^{-1/3}, \tag{10}$$

where the subscript 0 is used to represent the parameters for the base case (no HNO_3 in this study). For the condensation process, an increase in N_d is accompanied by an increase in the breadth of the droplet spectrum ($k/k_0 < 1$) so that the absolute change in r_e is moderated by the spectral broadening effect.

[15] The wavelength-dependent cloud optical depth is given by

$$\tau(\lambda) = \int_0^H \int_0^\infty \pi r^2 Q_{ext}(r, m, \lambda) n(r) dr dh, \tag{11}$$

where Q_{ext} is the extinction efficiency (a function of wavelength λ, r, and refractive index m), and H is the cloud geometric thickness. For an adiabatic cloud, the LWC is a linear function of height, $L = c_w h$, where c_w is the adiabatic condensation rate and h is the height relative to the cloud base. By using equations (4) and (9) and assuming N_d and k are constant in an adiabatic cloud, the cloud optical depth at visible wavelengths can be written as [e.g., *Boers and Mitchell*, 1994]

$$\tau = \frac{3}{5}\pi\overline{Q}_{ext}\left(\frac{3c_w}{4\pi\rho_w}\right)^{2/3}(kN_d)^{1/3}H^{5/3}. \tag{12}$$

For adiabatic clouds, assuming cloud LWC and H are not changed by the increase in N_d, the change in τ can be related to changes in N_d and k as

$$\frac{\tau}{\tau_0} = \left(\frac{k}{k_0}\right)^{1/3}\left(\frac{N_d}{N_{d0}}\right)^{1/3}. \tag{13}$$

Similar to the change in r_e, the change in τ will be moderated by spectral broadening ($k/k_0 < 1$).

[16] The cloud albedo can be calculated based on the simple expression by *Bohren* [1987]

$$A = \frac{(1-g)\tau}{2 + (1-g)\tau}, \tag{14}$$

where g is the scattering asymmetry factor ($\cong 0.84$). By using equation (13), the change in cloud albedo A due to changes in N_d and k can be calculated as

$$\frac{A}{A_0} = \left(\frac{k}{k_0}\right)^{1/3}\left(\frac{N_d}{N_{d0}}\right)^{1/3}\frac{2 + (1-g)\tau_0}{2 + (1-g)\tau_0\left(\frac{k}{k_0}\right)^{1/3}\left(\frac{N_d}{N_{d0}}\right)^{1/3}}. \tag{15}$$

[17] Spectral broadening associated with the change in N_d also affects the cloud susceptibility, which was originally defined by *Twomey* [1991] as

$$S_N \equiv \frac{dA}{dN_d} = \frac{A(1-A)}{3N_d}, \tag{16}$$

for a constant spectral breadth. To account for the spectral broadening effect, the cloud susceptibility can be written as

$$S \equiv \frac{dA}{dN_d} = \frac{A(1-A)}{3N_d} + \frac{A(1-A)}{3k}\frac{dk}{dN_d} = S_N\left(1 + \frac{d\ln k}{d\ln N_d}\right). \quad (17)$$

This equation shows that when spectral broadening is associated with increasing N_d, S_N is the upper limit for cloud susceptibility. When broadening is accompanied by processes that reduce N_d, S_N is a lower limit for cloud susceptibility (see similar analysis in *Feingold et al.* [1997]).

3. Results and Discussion

3.1. Growth Characteristics

[18] An adiabatic parcel model is used to simulate the activation and growth of hygroscopic aerosol under constant updrafts ($w = 0.1 \sim 1.0$ m s^{-1}). The initial air temperature is 15 °C, the pressure is 919 mb, and the relative humidity is 85%. The initial gas-phase HNO_3 concentrations are 1 and 5 ppb. The aerosol particles are composed of ammonium sulfate and assumed to have a lognormal size distribution over the radius range 0.01 ~ 1.1 μm with various number concentrations ($N_a = 50 \sim 1000$ cm^{-3}), median radii ($r_g = 0.05 \sim 0.12$ μm), and geometric standard deviations ($\sigma_g = 1.4 \sim 1.8$); a collection of 180 aerosol size distributions are used in this study. The aerosol/droplet population is divided into 20 discrete Lagrangian mass classes. Particle growth is calculated explicitly based on equations (2) and (3) using an ordinary differential equation solver. The mass accommodation coefficients of water and HNO_3 are respectively 0.042 [*Chodes et al.*, 1974] and 0.1 [*Xue*, 2002], while the thermal accommodation coefficient is 1.0 in the model [*Pruppacher and Klett*, 1997, p. 166]. (Sensitivity to the water mass accommodation coefficient is tested in section 3.3 by using a value of 1.0.) Water activity is calculated from the thermodynamic model developed by *Clegg et al.* [1998]. Collision-coalescence is not simulated. Simulations of cloud formation without HNO_3 are considered to be the "base cases".

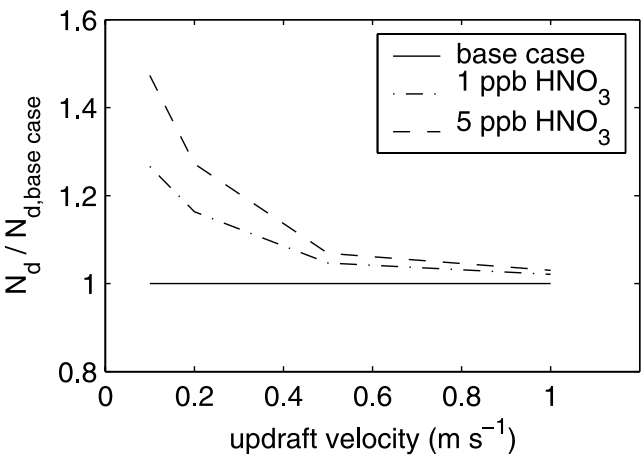

Figure 1. Cloud top N_d under different HNO_3 levels normalized to the base case (no HNO_3). The HNO_3 effect is most pronounced at low updrafts. At higher updrafts the supersaturation itself is high enough to activate a large fraction of aerosol. Aerosol parameters are $N_a = 200$ cm^{-3}, $r_g = 0.06$ μm, and $\sigma_g = 1.8$.

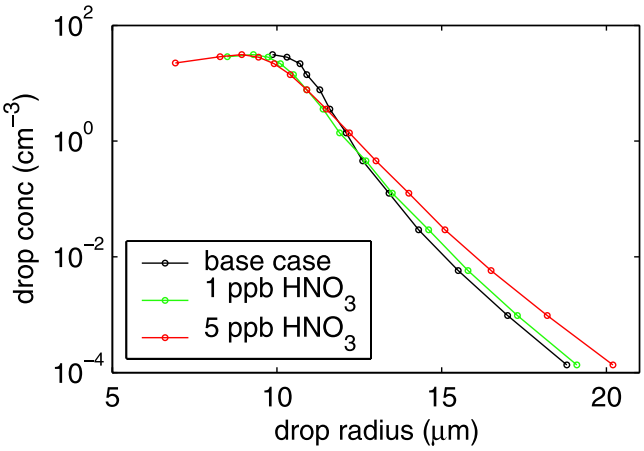

Figure 2. Cloud top droplet spectra for three simulations, under different HNO_3 levels at $w = 0.1$ m s^{-1} as illustrated in Figure 1. The spectral dispersions for the base case, $HNO_3 = 1$ ppb, and $HNO_3 = 5$ ppb are 0.052, 0.086, and 0.135, respectively.

[19] Figure 1 shows N_d under different HNO_3 levels when normalized to the respective base cases. The parameters of the aerosol size distribution in these simulations are $N_a = 200$ cm^{-3}, $r_g = 0.06$ μm, and $\sigma_g = 1.8$. N_d is evaluated at cloud top (~ 250 m above cloud base) where LWC = 0.5 g m^{-3}. It should be noted that cloud droplets in this study are referred to as droplets with radii larger than 1 μm although some of them may not be activated in the theoretical sense and may evaporate later. Droplets with large enough radii will contribute to the scattering of light whether they are activated or not. It can be seen in Figure 1 that the effect of HNO_3 on the formation of cloud droplets is most pronounced for weak updrafts. Similar results can be seen in *Kulmala et al.* [1993] and *Nenes et al.* [2002]. When $w = 0.1$ m s^{-1}, N_d is increased by about 30% with 1 ppb HNO_3 and 50% with 5 ppb HNO_3. For higher updrafts, HNO_3 no longer plays an important role in droplet formation because the high supersaturation itself can activate a large fraction of aerosol. Because the previous studies and this study all show no effect of HNO_3 on N_d at higher updrafts, we concentrate on low w and hereafter only show results at $w = 0.1$ m s^{-1}. Such updrafts are typical of weakly forced clouds such as stratus and stratocumulus.

[20] Figure 2 shows the droplet spectra at cloud top for the three simulations at $w = 0.1$ m s^{-1} in Figure 1. Increasing the HNO_3 concentration not only results in a higher N_d, but also a broader spectrum at both the small- and large-size ends. The relative dispersion D (defined as the standard deviation divided by the mean radius of the size spectrum) increases from 0.052 for the base case to 0.135 for the case with 5 ppb HNO_3.

[21] Figure 3a shows the time series of droplet sizes for the base case and the case with 5 ppb HNO_3 as shown in Figure 2 ($N_a = 200$ cm^{-3}, $r_g = 0.06$ μm, $\sigma_g = 1.8$). Simulation results prior to $t = 2500$ s are not shown because

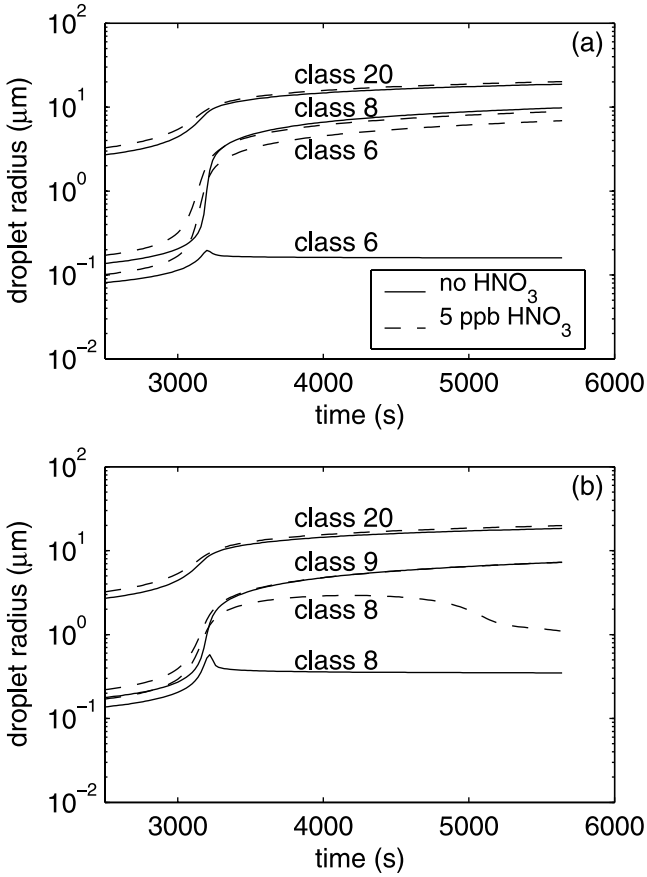

Figure 3. Two examples of the time series of droplet sizes at $w = 0.1$ m s^{-1}. (a) $N_a = 200$ cm^{-3}, $r_g = 0.06$ μm, and $\sigma_g = 1.8$. Class 8 is the smallest activated droplet size without HNO_3, while class 6 is the smallest activated size when $HNO_3 = 5$ ppb. (b) $N_a = 300$ cm^{-3}, $r_g = 0.08$ μm, $\sigma_g = 1.8$. Class 9 is the smallest activated size when $HNO_3 = 0$ ppb. With 5 ppb HNO_3, class 8 is activated and then deactivated due to the outgasing of HNO_3. Class 8 droplets are still counted as cloud droplets as long as their radii are larger than 1 μm.

droplet growth is slow during that stage. When HNO_3 is absent, size classes 8 to 20 are activated as cloud droplets. With 5 ppb HNO_3, classes 6 to 20 are activated. The two additional activated droplet classes lead to a broader spectrum at the small-size end. Figure 3b is another example of the time series of droplet sizes (N_a = 300 cm^{-3}, r_g = 0.08 μm, σ_g = 1.8). A distinct feature in Figure 3b is the slow evaporation of class 8 in the presence of 5 ppb HNO_3 so that the droplet spectrum at the small-size end is significantly broadened. These droplets are not completely activated and begin to evaporate at some point (see below). Although the evaporation of small cloud droplets and the growth of big droplets at their expense (Ostwald ripening effect) can also occur under conditions without HNO_3, this process occurs more often when HNO_3 is present.

[22] To explain the evaporation of class 8 shown in Figure 3b, time series of the ambient vapor pressure of HNO_3 and at the surface of class 8 droplets are plotted in Figure 4a. Classes 7 and 9 are also plotted for comparison. Time series of the water saturation ratio (ambient and at the droplet surfaces) are shown in Figure 4b. It is well known that small drops adjust to ambient conditions faster than big drops. Hence, as the relative humidity of the air parcel increases and the cloud drops absorb H_2O and HNO_3, small drops have higher vapor pressures of H_2O and HNO_3 than big drops. The uptake of HNO_3 by haze droplets adds more solute and lowers their critical supersaturations. Upon activation, H_2O and HNO_3 are absorbed quickly into cloud droplets. The ambient HNO_3 vapor pressure drops dramatically and may be lower than the equilibrium HNO_3 vapor pressures over the surfaces of small drops. As can be seen in Figure 4a, outgasing of HNO_3 from class 7 begins at time t1, and class 8 starts to lose HNO_3 at time t2, whereas HNO_3 diffuses to class 9 throughout the simulation. The slower decrease of the ambient HNO_3 vapor pressure after t1 and its increase after t2 are respectively the results of HNO_3 outgasing from class 7 and class 8 droplets. While losing HNO_3, the equilibrium water saturation ratio over the droplet surface increases and may be higher than the ambient water saturation ratio (see time > t3 in Figure 4b, for class 8 droplets), leading to the deactivation of the droplets.

[23] The increase in the activated droplet number by HNO_3 and the slow evaporation of the deactivating cloud droplets due to HNO_3 outgasing explain the spectral broad-

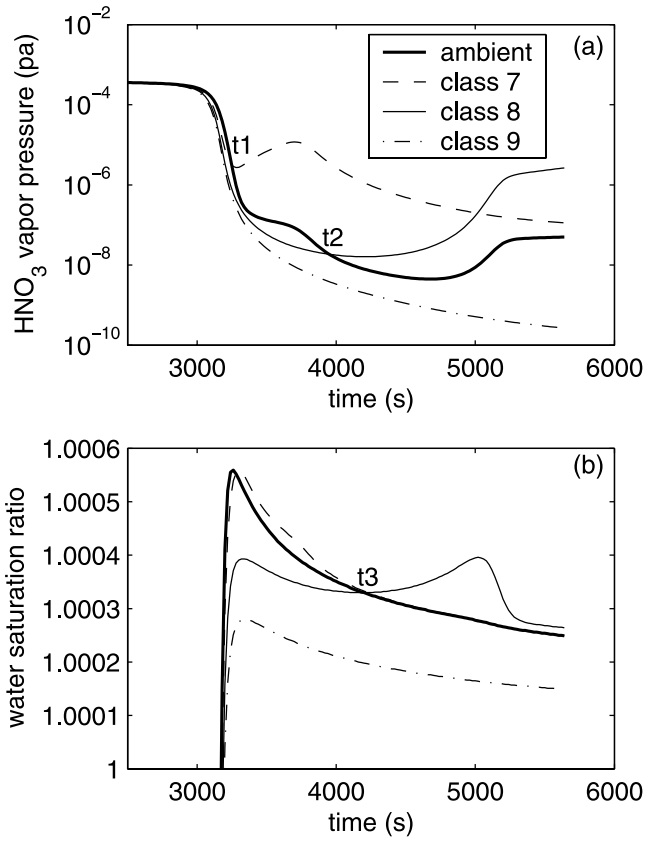

Figure 4. (a) Time series of the vapor pressures of HNO_3 in the ambient air, and over the droplet surfaces of three size classes at 5 ppb HNO_3. Aerosol parameters are N_a = 300 cm^{-3}, $r_g = 0.08$ μm, $\sigma_g = 1.8$ (as in Figure 3b). (b) Time series of the water saturation ratio in the ambient air and over the droplet surfaces.

ening at the small-size end. This evaporation provides water vapor to other droplets in the spectrum and affects their growth. The physical mechanism for broadening at the large-size end can be seen in Figure 5. Figure 5a shows the ambient water saturation ratio with and without HNO_3 for the case in Figures 2 and 3a (N_a = 200 cm^{-3}, r_g = 0.06 μm, σ_g = 1.8). It is seen that 5 ppb HNO_3 reduces the ambient water saturation ratio significantly. At the same time, HNO_3 also reduces the equilibrium saturation ratio over the droplet surface. Because the driving force for droplet growth (or evaporation) is the difference between the saturation ratios in the ambient air and over the droplet surface, how fast the droplet grows will depend on how H_2O and HNO_3 are distributed among the polydisperse droplets and in the gas phase. Figures 5b–5d show the driving force for the growth of three droplet classes. It is seen that class 20 has a larger driving force when 5 ppb HNO_3 is present, which explains the broadening at the large-size end of the spectrum as shown in Figure 2. The driving force for class 14 is not changed much by HNO_3, while the driving force for class 8 is decreased by HNO_3, as expected from Figure 2. In general, the spectral broadening at both the small- and large-size ends when HNO_3 is present is the result of competition of H_2O and HNO_3 among the polydisperse droplets.

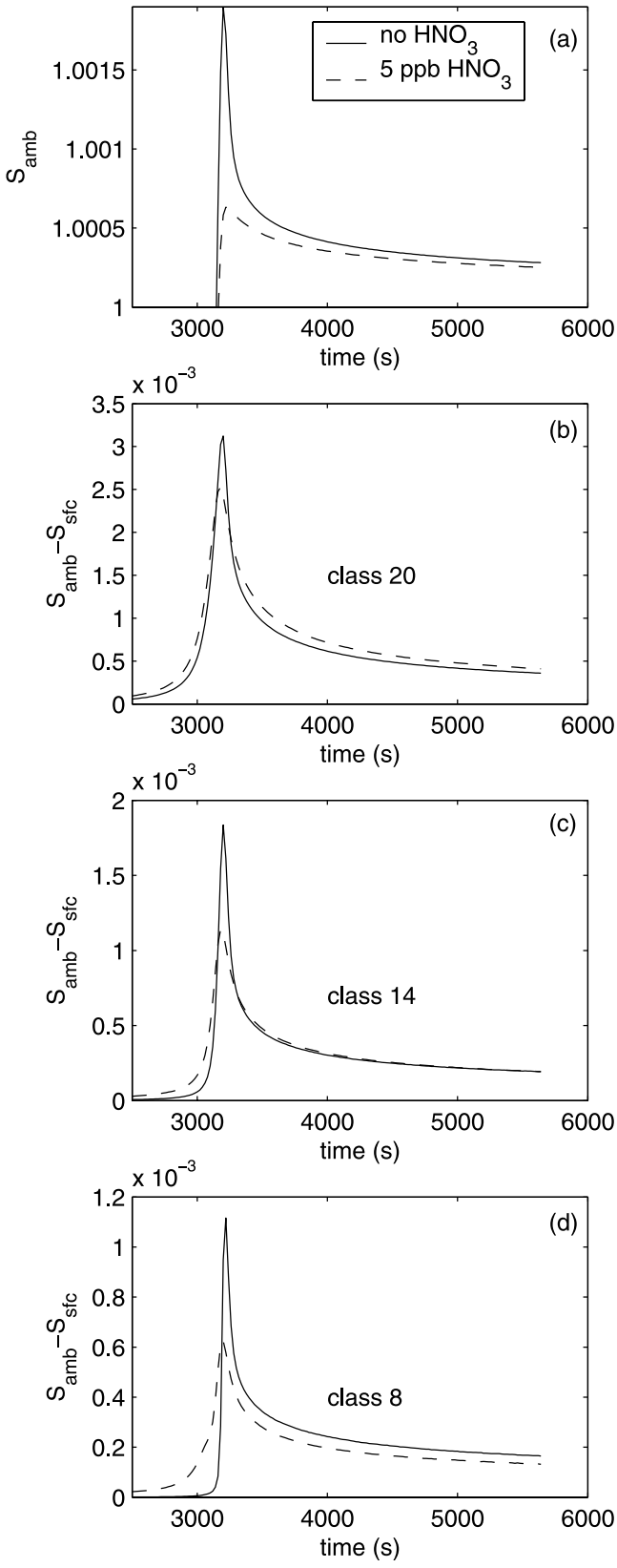

Figure 5. (a) Time series of the ambient water saturation ratio with and without HNO_3. HNO_3 reduces the ambient water saturation ratio by a significant amount. Aerosol parameters are N_a = 200 cm^{-3}, r_g = 0.06 μm, σ_g = 1.8 (as in Figure 3a). (b) Driving force ($S_{amb}-S_{sfc}$) for class 20 droplets. Compared to the results without HNO_3, class 20 has a larger driving force when HNO_3 = 5 ppb, which results in spectral broadening at the large-size end as shown in Figures 2 and 3a. (c) As in Figure 5b, but for class 14. (d) As in Figure 5b, but for class 8.

3.2. Optical Properties

[24] The changes in N_d and droplet spectra due to HNO_3 translate to modifications in cloud optical properties. The resultant changes in cloud optical properties due to 1 ppb HNO_3 are shown in Figure 6 for simulations with all 180 aerosol size distributions. The results are also compared to the theory in equations (10), (13), and (15) (for an adiabatic cloud) with and without the spectral broadening effect. Because r_e varies with height in an adiabatic cloud, this study only investigates the changes in cloud top r_e. As noted above, N_d may not be constant after the maximum supersaturation is achieved due to droplet deactivation. Similarly, D (and hence k) may also vary in a cloud. To evaluate the changes in cloud optical properties (τ, A, and cloud top r_e) in terms of the cloud microphysical properties (N_d and k), cloud top N_d and k (or D) are used in this study. Figure 6a shows the simulated results of τ/τ_0 as a function of $(N_d/N_{d0})^{1/3}$. It is seen that the modeled $(N_d/N_{d0})^{1/3}$ has a range of 1.0 ∼ 1.2 (implying an increase of 0 ∼ 70% in N_d) and that τ increases by 0 ∼ 14% when 1 ppb HNO_3 is present. However, the theory that ignores the spectral broadening effect (black line, $\tau/\tau_0 = (N_d/N_{d0})^{1/3}$) predicts an increase of 0 ∼ 19% in τ for this 0 ∼ 70% increase in N_d. The model results frequently diverge from the theory; the largest deviations are associated with the largest changes in spectral dispersion, as shown by the color coding and a few sample vertical lines in the figure. Figure 6b examines the model results of τ for the theory that includes the spectral broadening (black line, equation (13)). It can be seen that in

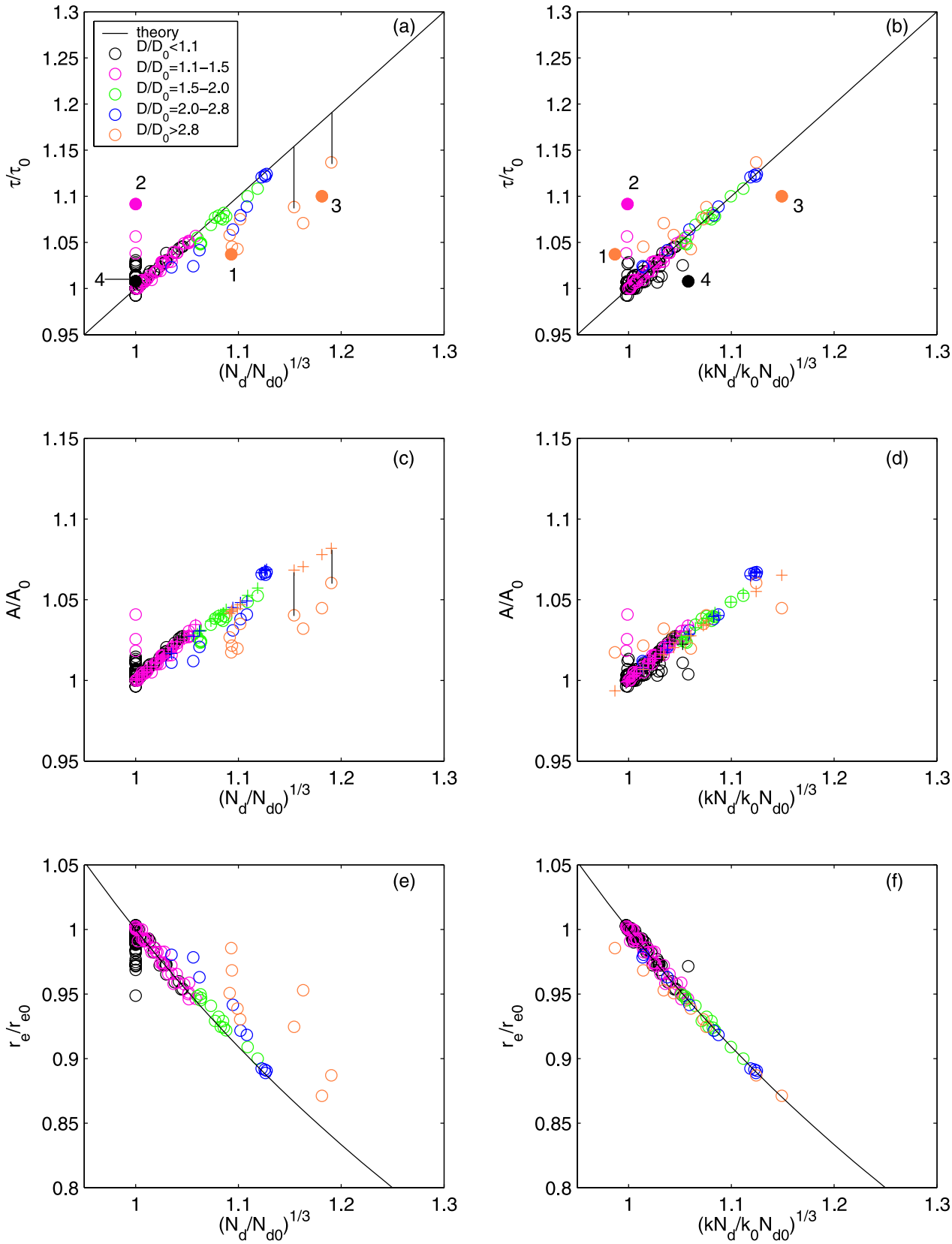
(a)
theory
D/D0<1.1
D/D0=1.1–1.5
D/D0=1.5–2.0
D/D0=2.0–2.8
D/D0>2.8
τ/τ0
(Nd/Nd0)1/3
(b)
(kNd/k0Nd0)1/3
(c)
A/A0
(d)
(e)
re/re0
(f)
1
2
3
4

Figure 6

general the results agree well with the theoretical line, indicating that equation (13) is a good parameterization of τ with N_d. The solid circles in Figures 6a and 6b that still deviate from the theoretical line after breadth changes are accounted for will be discussed below. Model results for the change in A are shown in Figures 6c and 6d as circles. The pluses in Figure 6c are calculated based on theory for each model run without the spectral broadening effect (equation (15) without the k/k_0 terms). It is seen that model results of A/A_0 deviate from the theory for some of the simulations. As shown by one of the vertical lines, the model calculates $A/A_0 = 1.03$ (an increase of 3% in A), while the theory predicts A/A_0 to be 1.06, i.e., double the increase in A. The pluses in Figure 6d are the theoretical calculations including the spectral broadening effect (equation (15)). The model results tend to agree with the pluses better, validating the use of equation (15) for estimating changes in A. Model results for the change in cloud top r_e are shown in Figures 6e and 6f. Similar to results for τ and A, model results for cloud top r_e deviate from the theory without the spectral broadening effect (black line in Figure 6e, $r_e/r_{e0} = (N_d/N_{d0})^{-1/3}$). After considering the broadening effect (black line in Figure 6f, equation (10)), the model results are in better agreement with the theory.

[25] Figure 7 shows the changes in cloud optical properties when 5 ppb HNO_3 is present. Modeled $(N_d/N_{d0})^{1/3}$ has a range of 1.0 $\sim$ 1.28 (an increase of 0 $\sim$ 110% in N_d) accompanied by an increase of 0 $\sim$ 20% in τ. This can be compared to increases of 0 $\sim$ 70% in N_d and 0 $\sim$ 14% in τ for HNO_3 = 1 ppb. Simulated clouds tend to have larger increases in dispersion compared to the case when HNO_3 = 1 ppb. This broadening counters the effects of an increase in N_d on τ, A, and r_e so that changes in optical properties are not as large as might have been expected by the effects of the five-fold increase in HNO_3 on N_d. Figure 7 shows again that the model results of cloud optical properties generally agree well with the theory that includes the spectral broadening effect.

[26] Although inclusion of the spectral broadening effect in the theory improves the agreement between the modeled cloud optical properties with theory, especially for cloud top r_e, there is still some discrepancy for τ and A (e.g., the solid circles in Figures 6a and 6b). The mechanism leading to the discrepancy is related to droplet deactivation, which changes N_d and k after the maximum supersaturation is achieved in an adiabatic cloud. As shown in Figure 3b, class 8 droplets are activated in the earlier stages of cloud evolution under 5 ppb HNO_3 but they deactivate due to the outgasing of HNO_3 at a later stage. The cloud top droplet spectra are then significantly broadened. Since τ is an integrated property over the cloud depth, applying the cloud top k in the parameterization can cause an over-correction to the theory (e.g., solid circle 1 in Figures 6a and 6b). In some cases, the deactivated droplets may evaporate to sizes smaller than 1 μm at cloud top and are not counted as cloud droplets. However, these droplets attain sizes large enough and for long enough in clouds so that they contribute to the scattering of light. This mechanism can result in an increase in τ by HNO_3 even though cloud top $N_d/N_{d0} = 1$ (e.g., solid circle 2 in Figures 6a and 6b). In addition, it should be noted that the deactivation of small cloud droplets may also occur in the base cases, where no HNO_3 is present. This is depicted in Figure 8 which shows the time series of droplet sizes with aerosol parameters of $N_a = 500$ cm^{-3}, $r_g = 0.06$ μm, $\sigma_g = 1.5$ (solid circle 3 in Figures 6a and 6b). It is seen that class 8 droplets are completely activated under 1 ppb HNO_3 whereas they deactivate to a size smaller than 1 μm when HNO_3 is absent. In this case, examination of cloud top N_d shows an increase in N_d by HNO_3. However, class 8 droplets still contribute to the scattering of light in the case without HNO_3 over a significant fraction of the cloud depth so that the optical depth between the two clouds is not as different as implied by the change in cloud top N_d, leading to the deviation of solid circle 3 from the theory. Solid circle 4 in Figures 6a and 6b represents a case where deactivated droplets in the base case sustain sizes larger than 1 μm at cloud top. In this case, they are counted as cloud droplets and the spectrum is significantly broadened. When using the cloud top k in the parameterization of τ, this significant cloud top spectral broadening in the base case can cause an over-correction to the theory. Thus, the changing N_d and k in an adiabatic cloud, which occur more often under the effect of HNO_3, impose a challenge for the parameterization of cloud optical properties. Averaging N_d and k over the entire cloud height might improve the agreement but we have not done so here. For the parameterization of cloud top r_e, the agreement between the model results and theory (equation (10)) is better than it is for τ and A because r_e, N_d, and k are all evaluated at cloud top.

[27] In summary, accounting for changes in spectral breadth significantly improves the agreement between model results and theory for effects on τ, A, and r_e related to HNO_3. When disagreements between model and theory do exist, they are related to variations in N_d and k over the depth of the cloud.

3.3. Sensitivity to the Mass Accommodation Coefficient of Water

[28] The mass accommodation coefficient of water α has been widely studied, with experimentally determined values ranging from 0.01 to 1 [e.g., *Chodes et al.*, 1974; *Wagner*, 1982; *Shaw and Lamb*, 1999; *Li et al.*, 2001]. The range of results indicates the difficulties of making precise measurements of α and the possible dependence of α on other physical parameters, such as temperature, pressure, and saturation ratio. Moreover, the range also indicates that

Figure 6. Cloud optical properties for HNO_3 = 1 ppb for all 180 aerosol size distributions. (a) Model results of τ/τ_0 versus $(N_d/N_{d0})^{1/3}$ compared to the theory that does not include the spectral broadening effect. (b) Model results of τ/τ_0 versus $(kN_d/k_0N_{d0})^{1/3}$ are compared to the theory that includes the spectral broadening effect (equation (13)). The solid circles are discussed in the text. (c) Model results of A/A_0 versus $(N_d/N_{d0})^{1/3}$. The pluses, which deviate from the model results, are the theoretical calculations based on equation (15) without the k/k_0 terms. (d) Model results of A/A_0 versus $(kN_d/k_0N_{d0})^{1/3}$. The pluses are calculated based on equation (15). (e) Model results of r_e/r_{e0} versus $(N_d/N_{d0})^{1/3}$ compared to the theory that does not include the spectral broadening effect. (f) Model results of r_e/r_{e0} versus $(kN_d/k_0N_{d0})^{1/3}$ compared to equation (10).

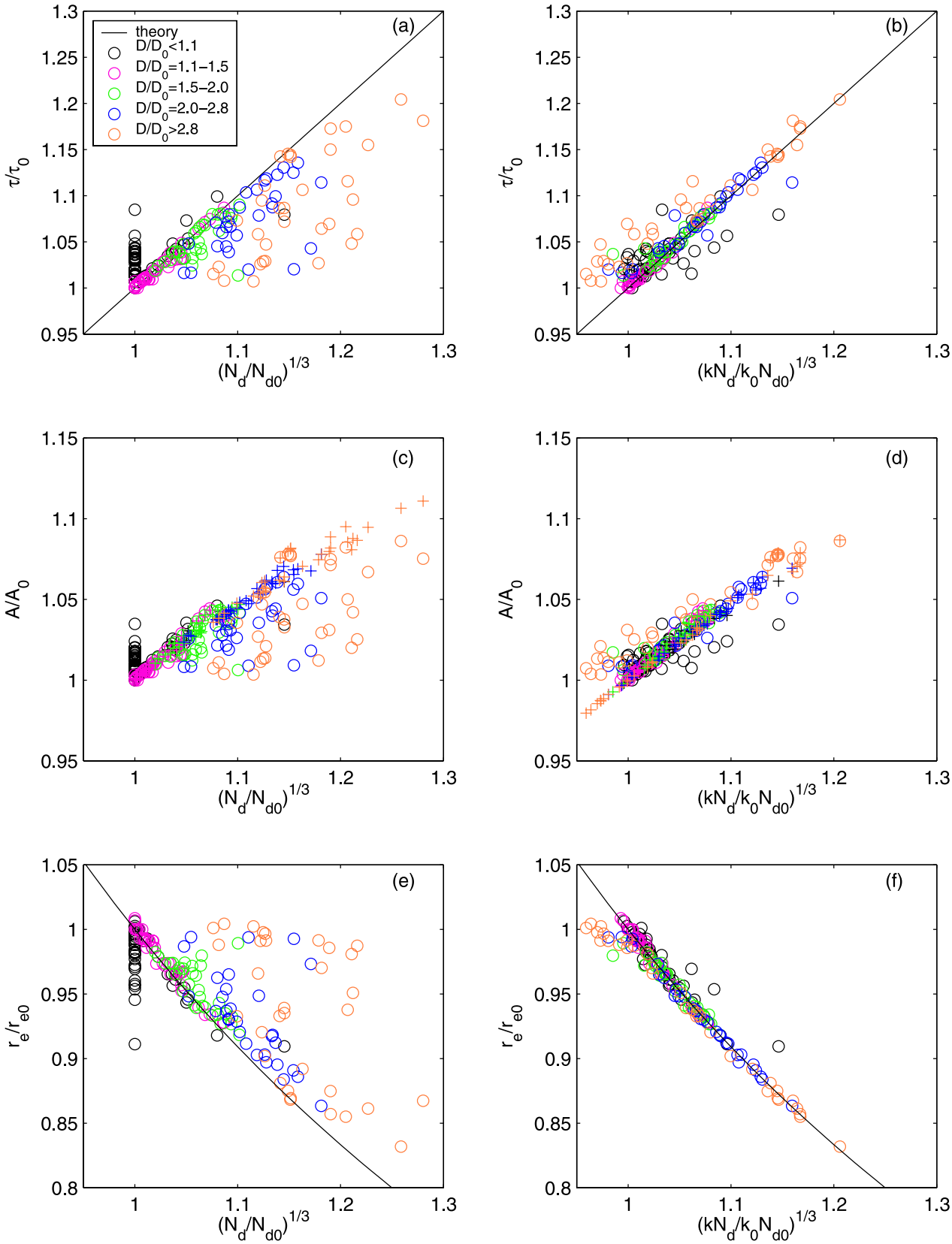

Figure 7. As in Figure 6, but for HNO_3 = 5 ppb.

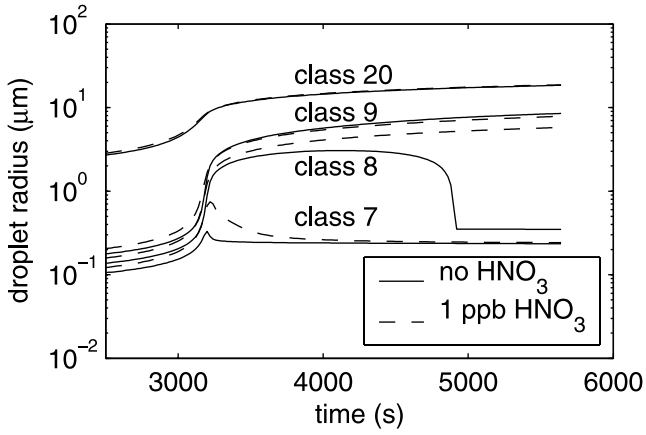

Figure 8. Time series of droplet sizes for an aerosol size distribution N_a = 500 cm^{-3}, r_g = 0.06 μm, σ_g = 1.5. This corresponds to the solid circle 3 in Figures 6a and 6b.

mechanisms of mass accommodation under different conditions might be different. Theoretically, α has been suggested to be unity from the viewpoint of collision theory [*Mozurkewich*, 1986]. However, based on classical nucleation theory, recent studies [e.g., *Li et al.*, 2001] have developed a two-step model that quantitatively resolves the temperature-dependence of α. They obtained a value of $\alpha = 0.17 \pm 0.03$ (at 280 K) with α inversely proportional to temperature.

[29] To investigate the sensitivity of model results to α, the simulations presented above ($\alpha = 0.042$) were repeated with $\alpha = 1$. Cloud optical properties for HNO_3 = 1 ppb compared to the base cases for all 180 aerosol size distributions are shown in Figure 9. (Model simulations with α = 1 and HNO_3 = 5 ppb were also performed but are not shown here. Their trends are qualitatively similar to the differences between the equivalent set of simulations at $\alpha = 0.042$.) It can be seen that 1 ppb HNO_3 results in a range of 1.0 $\sim$ 1.24 for $(N_d/N_{d0})^{1/3}$ (implying an increase of 0 $\sim$ 90% in N_d) and an increase of 0 $\sim$ 19% in τ. These results can be compared directly with Figure 6 ($\alpha = 0.042$) where increases in N_d and τ due to 1 ppb HNO_3 ranged from 0 $\sim$ 70% and 0 $\sim$ 14%, respectively. Thus HNO_3 has a stronger effect on droplet activation when $\alpha = 1$. The enhanced ability of HNO_3 to activate cloud droplets for higher α can be explained as follows. In the absence of HNO_3, higher α leads to faster condensation of water onto CCN, stronger competition for vapor and hence lower cloud supersaturation, and lower N_d. The presence of HNO_3 assists the activation of droplets, and therefore the potential for an increase in N_d (and an accompanying increase in dispersion D) is greater at the larger α. Figure 10 shows cloud top N_d for $\alpha = 1$ versus $\alpha = 0.042$ (no HNO_3) for all 180 aerosol size distributions. Although N_d is not always lower at the larger α, many cases (63%) do show such a trend. Decreases tend to occur more often at higher N_a, smaller r_g and smaller σ_g, but a detailed analysis is beyond the scope of this paper. Closer analysis of the results in Figure 9 also confirms that there are more cases of larger deviations in D from the base cases when $\alpha = 1$ than when $\alpha = 0.042$. For example, at 1 ppb HNO_3 there are 21 cases of $D/D_0 = 2.0-2.8$ when $\alpha = 1$ and only 10 when $\alpha = 0.042$. Conversely, there are 91 cases of $D/D_0 < 1.1$ when $\alpha = 1$ and 111 when $\alpha = 0.042$.

[30] More generally, and without attempting to arbitrate the value of α under ambient atmospheric conditions, the results indicate that the effects of HNO_3 on N_d and spectral breadth are not limited to small α, and tend to increase with increasing α. They also highlight the relative importance of accurate determination of α since differences in N_d due to a change in α may be similar in magnitude to differences due to HNO_3.

3.4. Caveats Regarding Possible Climate Impacts

[31] Although HNO_3 may be locally important for cloud formation, generalizing the parcel model results to the global scale requires consideration of numerous other factors.

[32] 1. HNO_3 concentrations: In this study, and other studies, the initial HNO_3 concentrations are typical of coastal and continental air. Over the open oceans, where stratocumulus clouds are prevalent and have the potential for strong radiative forcing because of the albedo contrast with the underlying ocean, the HNO_3 concentrations are usually several orders of magnitude lower than those needed to significantly change N_d. An exception is in ship tracks where HNO_3 may form from NO_x emissions and affect cloud formation [*Kulmala et al.*, 1993].

[33] 2. Updraft velocity: Results shown here are based on an updraft of 0.1 m s^{-1}, typical of stratiform clouds. However, the general effect on cloud optical properties should be derived from a convolution with the probability distribution function of the updraft velocities responsible for activation, as in *Feingold and Kreidenweis* [2000]. In cumulus clouds, where updrafts tend to be significantly higher, one would not anticipate an effect of HNO_3 on N_d.

[34] 3. Drop concentrations: Not all simulations result in an increase in N_d. For example, at 1 ppb HNO_3 and α = 0.042, only 85 of the 180 cases (47%) have $N_d/N_{d0} > 1$ (Figure 6). This value increases to 81% for 5 ppb HNO_3 and $\alpha = 0.042$ (Figure 7) and to 53% for HNO_3 = 1 ppb and $\alpha = 1$ (Figure 9). These numbers may be affected somewhat by the model size resolution. To test this, we ran numerous simulations at higher resolution (50 sizes) and found that, although there are sometimes quantitative differences between higher resolution simulations and the ones presented here, the qualitative differences described in this paper between simulations with and without nitric acid are robust. In addition, because the highest increases in N_d are accompanied by the largest increases in breadth, the effect of HNO_3 on cloud optical properties appears to be self-limiting.

[35] 4. Other effects: The effect of HNO_3 on clouds needs to be considered relative to other effects. Dynamical responses of the cloud system, particularly those that will result in larger cloud coverage, cloud lifetimes, or liquid water content have the potential to have a greater effect on the radiative forcing of clouds [*Feingold*, 2003].

[36] For the above mentioned reasons we hesitate to assess the global radiative forcing associated with HNO_3.

4. Conclusions

[37] Cloud parcel model results confirm that HNO_3 can increase droplet formation on ammonium sulfate aerosol particles but show for the first time that the associated drop

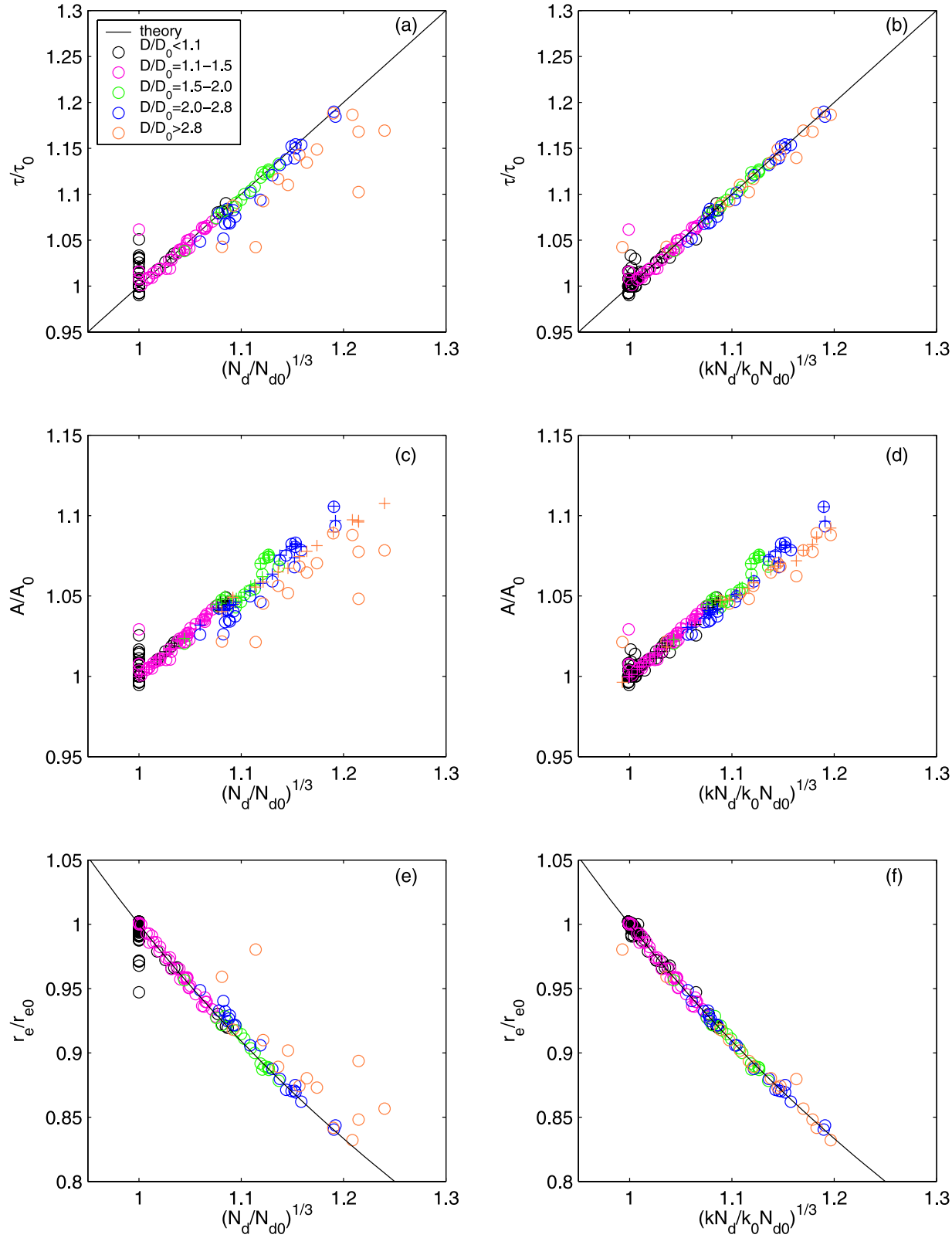

Figure 9. As in Figure 6, but for a water mass accommodation coefficient $\alpha = 1$.

spectral broadening tends to counter the effects of increased droplet concentrations on cloud optical properties, as represented by cloud optical depth, albedo, and cloud top effective radius for adiabatic clouds. As shown by previous workers [*Kulmala et al.*, 1993; *Nenes et al.*, 2002], and confirmed here, the effect is significant at low updraft velocities (~0.1 m s^{-1}) but minimal at high updrafts. Spectral broadening is shown to be caused by the compe-

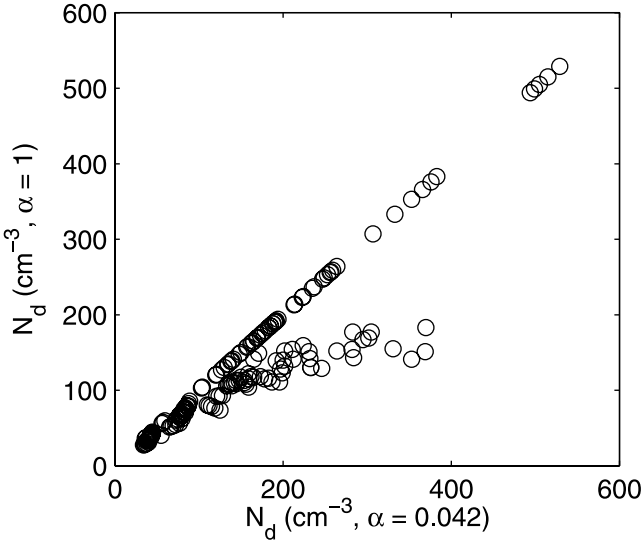

Figure 10. Comparison of cloud top activated droplet number concentration for $\alpha = 1$ versus $\alpha = 0.042$ in the absence of HNO_3.

tition for H_2O and HNO_3 by the polydisperse droplets under non-equilibrium conditions. Results show that higher HNO_3 concentrations do not necessarily lead to more reflective clouds according to simple theory, because the optical properties of clouds are not only related to the drop number concentration, but also to the spectral breadth. The broadening of the spectra tends to counter the cooling effect resulting from the increased drop number concentration. When spectral broadening effects are included, the parameterizations of cloud optical depth, albedo, and effective radius represent the cloud optical properties simulated from the parcel model for these adiabatic clouds reasonably well. When deviations do occur the reasons can be traced to situations where cloud drop concentrations and spectral breadths vary with height due to deactivation of droplets after the maximum supersaturation has been reached.

[38] Results have been obtained for two values of water vapor mass accommodation coefficient, $\alpha = 0.042$ and $\alpha = 1$, reflecting values commonly used in cloud models. We note that the increases in N_d and associated broadening of the drop spectrum are larger at the larger value of α. In addition we note that in the absence of HNO_3, drop concentrations calculated using $\alpha = 1$ are frequently much lower than those at $\alpha = 0.042$ (Figure 10) and that these differences are of similar order to the differences associated with HNO_3 concentrations on the order of a few ppb. Consensus on the appropriate value of α for ambient atmospheric conditions is therefore of great importance.

[39] It should be stressed that HNO_3 is only one of many factors affecting the nucleating properties of aerosols. Other aerosol size and composition related factors, as well as macroscale cloud properties such as cloud coverage, depth, lifetime, and liquid water content all need to be taken into account. For this, and other reasons, prediction of the radiative forcing by clouds remains an elusive goal.

[40] **Acknowledgments.** The authors would like to thank Simon Clegg for providing the code for the thermodynamic model. Helpful discussions with Barbara Ervens and Dennis Lamb are appreciated. Huiwen Xue acknowledges the National Research Council for a postdoctoral fellowship. Graham Feingold acknowledges support from NOAA's Climate and Global Change Research Program.

References

Ackerman, A. S., O. B. Toon, J. P. Taylor, D. W. Johnson, P. V. Hobbs, and R. J. Ferek (2000), Effects of aerosols on cloud albedo: Evaluation of Twomey's paramerization of cloud susceptibility using measurements of ship tracks, *J. Atmos. Sci.*, *57*, 2684–2695.

Albrecht, B. (1989), Aerosols, cloud microphysics, and fractional cloudiness, *Science*, *245*, 1227–1230.

Boers, R., and R. M. Mitchell (1994), Absorption feedback in stratocumulus clouds: Influence on cloud top albedo, *Tellus, Ser. A*, *46*, 229–241.

Bohren, C. F. (1987), Multiple scattering of light and some of its observable consequences, *Am. J. Phys.*, *55*, 524–533.

Charlson, R. J., S. E. Schwartz, J. M. Hales, R. D. Cess, J. A. Coakley Jr., J. E. Hansen, and D. J. Hofmann (1992), Climate forcing by anthropogenic aerosols, *Science*, *255*, 423–430.

Charlson, R. J., J. H. Seinfeld, A. Nenes, M. Kulmala, A. Laaksonen, and M. C. Facchini (2001), Reshaping the theory of cloud formation, *Science*, *292*, 2025–2026.

Chodes, N., J. Warner, and A. Gagin (1974), A determination of the condensation coefficient of water from the growth rate of small cloud droplets, *J. Atmos. Sci.*, *31*, 1351–1357.

Clegg, S. L., P. Brimblecombe, and A. S. Wexler (1998), Thermodynamic model of the system H^+-NH^+-SO_4^{2-}-NO_3^--H_2O at tropospheric temperatures, *J. Phys. Chem. A*, *102*, 2137–2154.

Facchini, M. C., M. Mircea, S. Fuzzi, and R. J. Charlson (1999), Cloud albedo enhancement by surface-active organic solutes in growing droplets, *Nature*, *401*, 257–259.

Feingold, G. (2003), Modeling of the first indirect effect: Analysis of measurement requirements, *Geophys. Res. Lett.*, *30*(19), 1997, doi:10.1029/2003GL017967.

Feingold, G., and P. Y. Chuang (2002), Analysis of the influence of film-forming compounds on droplet growth: Implications for cloud microphysical processes and climate, *J. Atmos. Sci.*, *59*, 2006–2018.

Feingold, G., and S. M. Kreidenweis (2000), Does cloud processing of aerosol enhance droplet concentration?, *J. Geophys. Res.*, *105*, 24,351–24,361.

Feingold, G., R. Boers, B. Stevens, and W. R. Cotton (1997), A modeling study of the effect of drizzle on cloud optical depth and susceptibility, *J. Geophys. Res.*, *102*, 13,527–13,534.

Gerber, H. (1996), Microphysics of marine stratocumulus clouds with two drizzle modes, *J. Atmos. Sci.*, *53*, 1649–1662.

Hegg, D. A. (2000), Impact of gas-phase HNO_3 and NH_3 on microphysical processes in atmospheric clouds, *Geophys. Res. Lett.*, *27*, 2201–2204.

Hoppel, W. A., G. M. Frick, J. W. Fitzgerald, and R. E. Larson (1994), Marine boundary layer measurements of new particle formation and the effects nonprecipitating clouds have on aerosol size distribution, *J. Geophys. Res.*, *99*, 14,443–14,459.

Hudson, J. G., and S. S. Yum (1997), Droplet spectral broadening in marine stratus, *J. Atmos. Sci.*, *54*, 2642–2654.

Kulmala, M., A. Laaksonen, P. Korhonen, T. Vesala, T. Ahonen, and J. C. Barrett (1993), The effect of atmospheric nitric acid vapor on cloud condensation nucleus activation, *J. Geophys. Res.*, *98*, 22,949–22,958.

Kulmala, M., P. Korhonen, A. Laaksonen, and T. Vesala (1995), Changes in cloud properties due to NO_x emissions, *Geophys. Res. Lett.*, *22*, 239–242.

Kulmala, M., P. Korhonen, T. Vesala, H. C. Hansson, K. Noone, and B. Svenningsson (1996), The effect of hygroscopicity on cloud droplet formation, *Tellus*, *Ser. B*, *48*, 347–360.

Kulmala, M., A. Laaksonen, R. J. Charlson, and P. Korhonen (1997), Clouds without supersaturation, *Nature*, *388*, 336–337.

Laaksonen, A., P. Korhonen, M. Kulmala, and R. J. Charlson (1998), Modification of the Köhler equation to include soluble trace gases and slightly soluble substances, *J. Atmos. Sci.*, *55*, 853–862.

Li, Y. Q., P. Davidovits, Q. Shi, J. T. Jayne, C. E. Kolb, and D. R. Worsnop (2001), Mass and thermal accommodation coefficients of H_2O(g) on liquid water as a function of temperature, *J. Phys. Chem. A*, *105*, 10,627–10,634.

Liu, Y., and P. H. Daum (2002), Indirect warming effect from dispersion forcing, *Nature*, *419*, 580–581.

Martin, G. M., D. W. Johnson, and A. Spice (1994), The measurement and parameterization of effective radius of droplets in warm stratocumulus clouds, *J. Atmos. Sci.*, *51*, 1823–1842.

McFarquhar, G. M., and A. J. Heymsfield (2001), Parameterizations of INDOEX microphysical measurements and calculations of cloud suscept-

ibility: Applications for climate studies, *J. Geophys. Res.*, *106*, 28,675–28,698.
Mozurkewich, M. (1986), Aerosol growth and the condensation coefficient for water: A review, *Aerosol Sci. Technol.*, *5*, 223–236.
Nenes, A., R. J. Charlson, M. C. Facchini, M. Kulmala, A. Laaksonen, and J. H. Seinfeld (2002), Can chemical effects on cloud droplet number rival the first indirect effect?, *Geophys. Res. Lett.*, *29*(17), 1848, doi:10.1029/2002GL015295.
Peng, Y., and U. Lohmann (2003), Sensitivity study of the spectral dispersion of the cloud droplet size distribution on the indirect aerosol effect, *Geophys. Res. Lett.*, *30*(10), 1507, doi:10.1029/2003GL017192.
Pruppacher, H. R., and J. D. Klett (1997), *Microphysics of Clouds and Precipitation*, 954 pp., Kluwer Acad., Norwell, Mass.
Rosenfeld, D. (2000), Suppression of rain and snow by urban and industrial air pollution, *Science*, *287*, 1793–1796.
Schwartz, S., E. Harshvardhan, and C. M. Benkovitz (2002), Influence of anthropogenic aerosol on cloud optical depth and albedo shown by satellite measurements and chemical transport modeling, *Proc. Natl. Acad. Sci.*, *99*, 1784–1789.
Seinfeld, J. H., and S. N. Pandis (1998), *Atmospheric Chemistry and Physics*, 1326 pp., John Wiley, Hoboken, N. J.
Shaw, R. A., and D. Lamb (1999), Experimental determination of the thermal accommodation and condensation coefficients of water, *J. Chem. Phys.*, *111*, 10,659–10,663.
Twomey, S. (1974), Pollution and the planetary albedo, *Atmos. Environ.*, *8*, 1251–1256.
Twomey, S. (1977), The influence of pollution on the shortwave albedo of clouds, *J. Atmos. Sci.*, *34*, 1149–1152.
Twomey, S. (1991), Aerosols, clouds, and radiation, *Atmos. Environ.*, *25*, 2435–2442.
Wagner, P. E. (1982), Aerosol growth by condensation, in *Aerosol Microphysics*, vol. 2, *Chemical Physics of Microparticles*, edited by W. H. Marlow, pp. 129–178, Springer-Verlag, New York.
Xue, H. (2002), Experimental studies of the evaporation and growth of individual aqueous droplets, Ph.D. thesis, 121 pp., Pa. State Univ., University Park.
Zou, Y.-S., and N. Fukuta (1999), The effect of diffusion kinetics on the supersaturation in clouds, *Atmos. Res.*, *52*, 115–141.

G. Feingold and H. Xue, Environmental Technology Laboratory, NOAA, 325 Broadway, Boulder, CO 80305, USA. (huiwen.xue@noaa.gov)